ARTICLE OPEN

Check for updates

Miniaturized multicolor fluorescence imaging system integrated with a PDMS light-guide plate for biomedical investigation

Hyogeun Shin[1,9], Gun-Wook Yoon[2,9], Woongsun Choi[3,8], Donghwan Lee[4], Hoyun Choi[4], Deok Su Jo[5], Nakwon Choi[3,6]✉, Jun-Bo Yoon[2]✉ and Il-Joo Cho[1,7]✉

Miniaturized fluorescence imaging systems are promising platforms that overcome the limited use of conventional microscopes in the biomedical field. However, there are physical limitations for multicolor fluorescence imaging in existing miniaturized imaging systems because multiple filters have to be integrated into a small structure. Here, we present a miniaturized multicolor fluorescence imaging system integrated with single polydimethylsiloxane (PDMS) light-guide plate (LGP) for multicolor fluorescence imaging. The PDMS LGP allows guiding the transmitted light from the light source only to the fluorescent samples regardless of the wavelength of the light source. Thus, our system is capable of multicolor fluorescence imaging without multiple filters that block the excitation light. We demonstrated the usability of our system in the biomedical field by observing green- and red-labeled cells in the incubator. Our proposed system can be used in a wide range of applications for studies that require multicolor fluorescence imaging in the biomedical field.

npj Flexible Electronics (2023)7:7 ; https://doi.org/10.1038/s41528-023-00243-6

INTRODUCTION

Observation of dynamic changes in living cells is essential for studying various physiological processes, such as cell differentiation and proliferation processes[1]. Specifically, the differentiation process could be understood through continuous observation of the morphological changes in cells[2]. For example, the increase of cell body or length of the neurites is the morphological characteristic during the development of induced pluripotent stem cells (iPSCs) into neurons[3]. As such, for observing the dynamic changes in living cells that can provide in-depth information on the physiological process, a stable and controlled culture environment must be provided. The ideal approach would be to monitor the cells through a fluorescence microscope in a CO_2 incubator. Although the most widely used conventional fluorescence microscope allows observation of subcellular structures in the cells (e.g., nucleus and cytoskeleton) with high spatial resolution, it is difficult to put the microscope in the incubator due to its bulky size[4–8]. Thus, a customized incubating system is required to continuously monitor living cells. Also, to overcome the intrinsic low field-of-view (FOV) of lens-based microscopes, a motorized stage for precise and fast stage movement is required[4–8]. The fluorescence microscopes that incorporate the customized incubating system and the motorized stage have enabled continuous monitoring of the cells in a large area. However, the system's complexity has been increased by integrating multiple mechanical and electronic devices, such as temperature and humidity modules, a customized chamber, a motorized stage, and control devices. Also, user accessibility has been limited due to the additional costs associated with adding multiple devices.

Recent developments in miniaturized lensless fluorescence imaging systems have overcome the limitations of integrating fluorescence microscopes with the incubating system[4–14]. Handheld-size fluorescence imaging systems can provide continuous monitoring of cells inside an incubator with a spatial resolution of about ten micrometers[4,7]. Such systems have a compactly built-in light source (e.g., small LED) for the excitation of fluorescent samples and they have a fluorescent filter (e.g., absorption filter) for blocking directly transmitted light from the light source to the light detector (e.g., image sensor). Such compact configurations enable us to observe the emission light from the fluorescent samples, such as labeled cells, even in a small size. Also, by applying either a complementary metal-oxide-semiconductor (CMOS) or a charge-coupled device (CCD) image sensor array without a lens, miniaturized fluorescence imaging systems enable high throughput imaging through a large FOV that is 10 times higher compared to conventional fluorescence microscopes (FOV = 2 – 3 mm^2) with similar image resolution by image processing algorithms[10,15].

However, previous miniaturized fluorescence imaging systems were limited to single-color fluorescence imaging because of difficulties in integrating multiple filters. Multicolor fluorescence imaging systems have a wider range of applications, for example, simultaneous multi-type cell monitoring and quantifying multiple disease biomarkers[16–18]. One imaging system that was developed recently adapted the exchange of two optical filters for multicolor fluorescence imaging. It could successfully observe, for example, human breast cancer cells labeled in two colors through a manual exchange of the optical filters[19]. Another imaging system used a

[1]Department of Biomedical Sciences, College of Medicine, Korea University, Seoul, Republic of Korea. [2]School of Electrical Engineering, Korea Advanced Institute of Science and Technology (KAIST), Deajeon, Republic of Korea. [3]Center for Brain Technology, Brain Science Institute, Korea Institute of Science and Technology (KIST), Seoul, Republic of Korea. [4]Biotechnology Research Institute of CHROMACH Co., Ltd, Suwon, Republic of Korea. [5]School of Chemical Engineering, Sungkyunkwan University (SKKU), Suwon, Republic of Korea. [6]KU-KIST Graduate School of Converging Science and Technology, Korea University, Seoul, Republic of Korea. [7]Department of Anatomy, College of Medicine, Korea University, Seoul, Republic of Korea. [8]Present address: Noul Co., Ltd, Yongin, Republic of Korea. [9]These authors contributed equally: Hyogeun Shin, Gun-Wook Yoon.
✉email: nakwon.choi@kist.re.kr; jbyoon@kaist.ac.kr; ijcho@korea.ac.kr

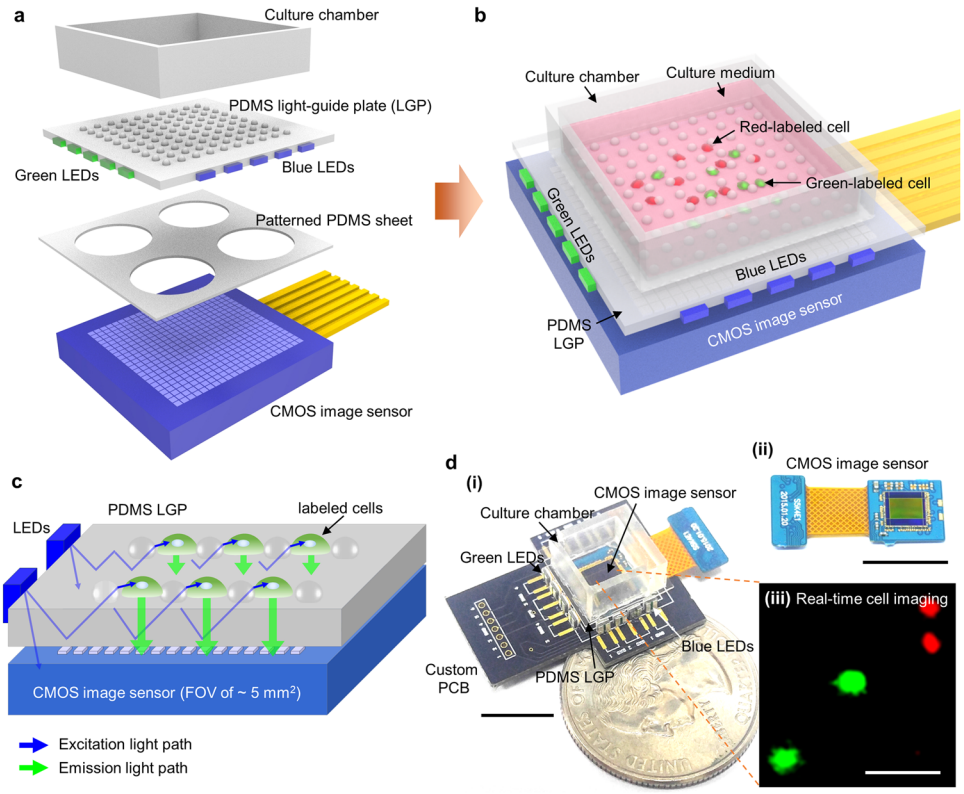

Fig. 1 Miniaturized multicolor fluorescence imaging system integrated with a PDMS LGP. a Schematic diagram of each component of the proposed system. **b** Schematic diagram of the packaged system with green- and red-labeled cells. **c** The simple operating principle of the proposed system. The light transmitted from the LEDs is transmitted only to the labeled cells due to total internal reflection (TIR) on the LGP's bottom surface, and the emission light from the labeled cells is transmitted to the CMOS image sensor. **d** Photographs of the packaged system, image sensor used, and example image showing the green- and red-labeled NIH 3T3 fibroblast cells using the proposed system. Scale bar: 10 mm (**d**-i, ii) 50 μm (**d**-iii).

smartphone-based, dual-band filter that was developed to observe targeted DNA sequencing reactions[20]. These systems adapted fluorescence filters for multicolor fluorescence imaging (e.g., multiple-filter set or a dual-band filter). Fluorescence filters are essential for fluorescence imaging, but integrating multiple fluorescence filters and switching modules into the limited size of a miniaturized system can complicate the system. Also, dual-band fluorescence filters make it challenging to observe more than two multiple fluorescence bands because the number of fluorescence bands is limited to two.

To enable multicolor imaging in a limited form factor, a light-guide plate (LGP) can be an substitute for multiple or dual-band fluorescence filters. The LGP, which is used as the backlight unit (BLU) of a liquid-crystal display, transmits light only in the direction of one plane by total internal reflection (TIR) irrespective of the wavelength of the light source. Therefore, the LGP can be used to guide excitation light from light sources to only fluorescent samples, and it can be used for multicolor fluorescence imaging.

In this study, we proposed a miniaturized, multicolor fluorescence imaging system using an LGP for multicolor fluorescence imaging (Fig. 1). The system was integrated with multicolor LEDs, a CMOS image sensor without a lens, and a polydimethylsiloxane (PDMS) LGP[21] instead of multiple or dual-band optical filters (Fig. 1a, b). Through the integration of only one PDMS LGP, we were able to observe multicolor fluorescent samples because the PDMS LGP transmitted excitation light only to fluorescent samples by TIR irrespective of wavelength (Fig. 1c). Also, the PDMS LGP with spherical light out-couplers uniformly spread the excitation light from the LEDs to fluorescent samples located on the PDMS LGP. We successfully demonstrated the feasibility of our proposed miniaturized, multicolor, fluorescence imaging system through observation of its dynamic characteristics, such as cell spreading, migration, and proliferation of green- or red-labeled NIH 3T3 fibroblast cells in an incubator. We expect our proposed system integrated with a PDMS LGP can be used in various studies on biomedical applications that require multicolor fluorescence imaging, such as multi-type cell monitoring and quantification of multiple disease biomarkers.

RESULTS

Principle of the operation of a miniaturized fluorescence imaging system integrated with PDMS LGP

For multicolor fluorescence imaging, we designed a fluorescence imaging system combined with PDMS LGP instead of using multiple filters or dual-band filters. The designed fluorescence imaging system consists of LEDs for excitation of fluorescent samples, image sensors for detection of the light emitted from fluorescent samples, and a PDMS LGP for guiding the light transmitted from LEDs to the fluorescent samples (Fig. 1). The principle of the operation of the proposed fluorescence imaging system can be explained through three steps (Fig. 2a). First, light illuminated from LEDs is transmitted to the side of the PDMS LGP. Second, the incidence light to the LGP is only transmitted to the top surface where the fluorescent samples are located; this is due to the optical properties of PDMS and the micropatterns of the top surface of the PDMS LGP. Specifically, total internal reflection (TIR) takes place at the boundary between the PDMS and the air when a ray of light inside the PDMS LGP approaches the air at an angle of incidence greater than the critical angle ($\theta_c = 44.3°$) because

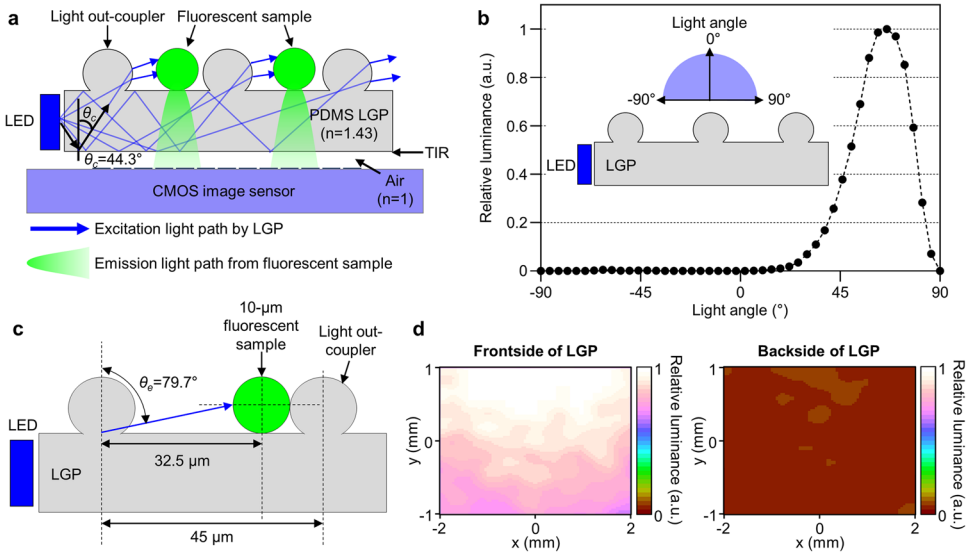

Fig. 2 Design and simulation results of the PDMS LGP. a Schematic diagram showing the overall configuration and operating principle of the fluorescence imaging system integrated with a PDMS LGP. θ_c is the critical angle. **b** Result of the simulation of the angular luminance distribution of PDMS LGP with spherical light out-couplers. **c** The maximum extracted angle of light (θ_e) from the light out-coupler based on 10-μm fluorescent sample located on the top surface of the PDMS LGP, where the height of the light out-coupler is 10 μm, the diameter of the light out-coupler is 15 μm, and the pitch of the light out-couplers is 45 μm. **d** Simulated spatial illumination distribution of (left) front and (right) back of the PDMS LGP.

PDMS (n = 1.43) has a higher refractive index than air ($n = 1$). In the proposed system, we enable only the transmission of light above the critical angle through the PDMS LGP by allowing the other ray of light to pass through the PDMS surface in the vicinity of the edge of the PDMS LGP. Thus, TIR takes place on the flat bottom surface of the PDMS LGP, so that light is not transmitted below the bottom surface. However, on the patterned top surface of the PDMS LGP, total internal reflection does not take place due to the spherical light out-couplers, which change the incidence angle of the light, so the rays of light go through the top surface of the PDMS LGP. Third, fluorescent samples located on the top surface are excited by the transmitted light from the top surface of the PDMS LGP, and the light emitted from the fluorescent samples is transmitted to the image sensor located below the PDMS LGP.

In summary, the proposed fluorescence imaging system has integrated PDMS LGP instead of fluorescence filters to transmit the excitation light from the LEDs only to the top surface of the PDMS LGP, where the fluorescent samples are located. Therefore, our system does not need fluorescence filters to block the excitation light from the LEDs, and it blocks all visible light regardless of its wavelength. Through this operation principle, the proposed system is capable of multicolor fluorescence imaging, in principle, above three colors by only integrating multicolor LEDs for the excitation of multicolor fluorescent samples, which is impossible to implement with multiband filters.

Design and optical simulation of the PDMS LGP

We designed and optimized the PDMS LGP for the uniform illumination of excitation light to samples on the LGP while minimizing the leakage of the excitation light to the CMOS image sensor under the LGP. The light emitted from LEDs is guided inside the LGP by TIR and radiated from the top surface of the LGP through the light out-couplers. Accordingly, the optical properties of the LGP are related strongly to the shape, dimensions, and density of the light out-couplers.

First, we designed the shape of the light out-couplers so that light could be transmitted to fluorescent samples positioned on top of the LGP between the light out-couplers. The traditional LGP used in BLU of LCD had light out-couplers of inverse-trapezoidal shape, which transmit most of the light in a vertical direction[22]. Therefore, this structure is not suitable for transmitting light to the fluorescent sample positioned between the couplers. However, the spherical light out-couplers transmit a relatively large amount of light in the horizontal direction due to their curved surfaces (Fig. 2a).

Next, we optimized the dimensions of the spherical light out-couplers. According to previous studies, larger light out-couplers induced the transmission of more light to the samples on the LGP[21]. However, the dimensions of the light out-couplers depend on the size of the fluorescent sample to be observed. For example, if the sample is much smaller than the light out-coupler, it is difficult to deliver the light to the samples (Supplementary Fig. 1a) because the angle of light from the light out-coupler is smaller than 90°. To observe cells that are used mostly in the biomedical field (typically 10–20 μm)[23], we decided that the height of the light out-couplers should be 10 μm and their diameters should be 15 μm, making them similar to the size of the cells. Also, to predict the relative amount of light transmitted according to the angle of light from the light out-coupler, we used a LightTools® optical simulator with core and illumination modules (LightTools® optical simulator 8.4.0, Synopsys, Mountain View, CA, USA) to simulate the angular luminance distribution of the LGP with spherical light out-couplers that were 10 μm high and had diameters of 15 μm. The simulation result showed a wide and large light extraction angle (45° − 85°), which is sufficient for the transmission of the light to the fluorescent samples positioned between the light couplers (Fig. 2b).

We also decided on the packing density of the light out-couplers for minimum light distortion and uniform light transmission. The high density induces a low fill factor of samples on the LGP because it would be difficult to locate samples on the light out-couplers due to light distortion (Supplementary Fig. 1b). However, if the density of the light out-couplers is low, light may not be transmitted according to samples far from the light out-couplers (Supplementary Fig. 1c). To optimize the density of the light out-couplers, we considered the light extraction angle (i.e., 45°−85° based on the simulation result) so that we could deliver light to the 10 μm fluorescent sample, which is similar to the cell size between the couplers (Fig. 2c and Supplementary Fig. 1d and

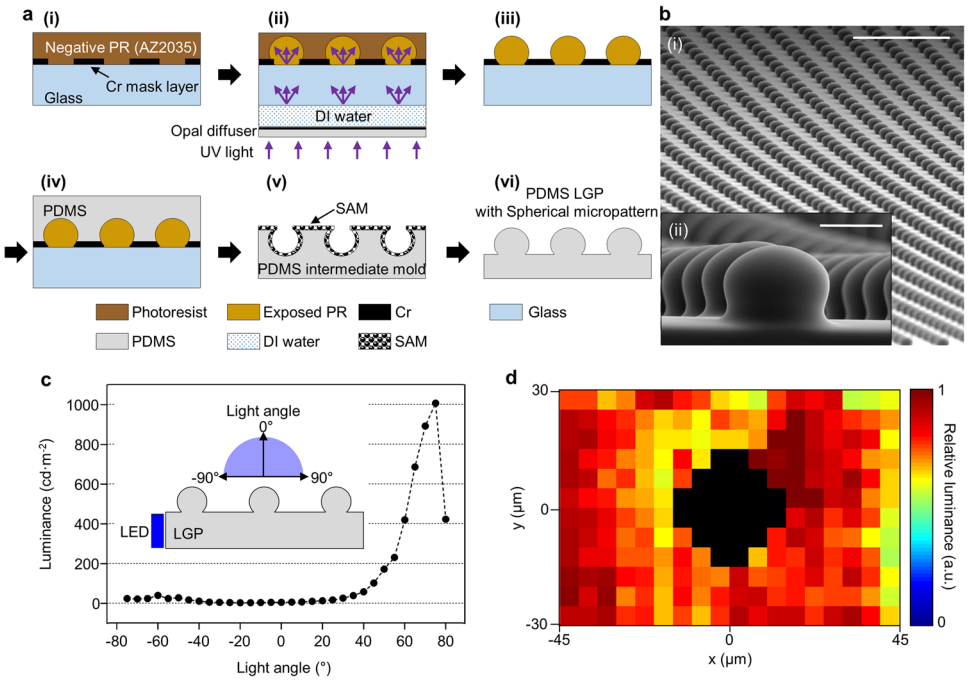

Fig. 3 Fabrication and characterization of the PDMS LGP with spherical light out-coupler. a The fabrication process for the proposed PDMS LGP: (i) negative photoresist coating on the patterned Cr layer, (ii) backside diffuser lithography, (iii) photoresist mold after development, (iv) liquid PDMS coating and curing, (v) replication of the intermediate mold and self-assembled monolayer coating, and (vi) PDMS LGP replication. **b** Scanning electron microscopy image of the fabricated PDMS LGP. **c** Measured angular luminance distributions of the fabricated PDMS LGP. **d** luminance distribution around the light out-coupler based on the measured result using 10-μm fluorescent beads. Scale bar: 100 μm (**b**-i) 10 μm (**b**-ii).

Supplementary Note. 1). Therefore, we designed the gap between the light out-couplers to be 45 μm, which was the maximum distance between the light out-coupler and a sample ensuring light transmission to the sample (i.e., the density of 8.72%) (Fig. 2c, Supplementary Fig. 1d, and Supplementary Note. 1). This light extraction angle of 79.7° is within the angle distribution of PDMS LGP (45° − 85°), which ensures that most of the light extracted from the light out-couplers can be delivered to the samples regardless of the position of the small fluorescent samples larger than 10 μm.

Finally, we simulated the relative amount of light transmitted from the front and from the back of the PDMS LGP using the LightTools® optical simulator to estimate the amount of light that leaked from the backside to the CMOS image sensor (Fig. 2d). In the simulation, we applied the optimized dimensions (i.e., light out-couplers that were 10 μm high, 15 μm in diameter, and had a pitch of 45 μm between them) with four LEDs at the edge of the LGP. In addition, the total size of the LGP was 12×12 mm^2 and its thickness was 100 μm. Also, the image sensor was positioned 5.5 mm from the side LEDs (same as the optical system used in the experiment). Also, the range of incident angle from the LED was set from −125° to +125°. As shown by optical simulation result from the area of 4×2 mm^2 where the image sensor was located, our PDMS LGP emitted <0.1% of light backward relative to the front (Fig. 2c). This value was low enough to measure the emission light from fluorescent samples while blocking the direct light to the CMOS image sensor. In conclusion, we confirmed that the designed PDMS LGP could sufficiently replace fluorescence filters in the miniaturized multicolor fluorescence imaging system.

Fabrication and characterization of the PDMS LGP

The fabrication process of the PDMS LGP is shown in Fig. 3a. Initially, we deposited a 200-nm-thick Cr layer on a soda-lime glass wafer and patterned a circular hole array using conventional photolithography. Next, we coated a 12-μm-thick negative photoresist AZ2035 (AZ Electronic Materials Ltd., Luxembourg) on the Cr layer. We performed backside diffuser lithography to make a photoresist master mold of the spherical light out-coupler array[24]. We used a commercial opal diffuser and deionized (DI) water as the index-matching liquid during diffuser lithography to control the shape of the light out-coupler[24]. After UV exposure and development, we poured PDMS on the photoresist mold and cured it to make an intermediate PDMS mold. Next, the surface of the intermediate PDMS mold was coated with a self-assembled monolayer (SAM) (CF_3-$(CF_2)_5(CH_2)_2SiCl_3$; Fluka) after the mold was treated with oxygen plasma for the adhesion enhancement with the SAM layer. To control the thickness of the PDMS LGP, liquid phase PDMS was spin-coated on the intermediate PDMS mold. Finally, the liquid PDMS was cured and peeled off from the intermediate PDMS mold. In this process, the SAM layer prevented the cured PDMS layer from bonding to the intermediate PDMS mod. We successfully fabricated the PDMS LGP with uniform light out-couplers on the surface (Fig. 3b). The height and diameter of each light out-coupler were 10 and 15 μm, respectively, and they were distributed evenly with the pitch of 45 μm on the LGP top surface for the enhancement of light uniformity.

On the side of the fabricated LGP, we attached four LEDs (blue XLamp XQ-E HI LED, Cree, Inc., Durham, NC, USA) and measured the angular luminance distribution of the fabricated PDMS LGP using a spectroradiometer (CS-2000, Konica Minolta, Osaka, Japan). Consistent with the simulation results, the angular luminance distribution showed a large light extraction angle of ~75° (Fig. 3c), which ensures that the light emitted from the light out-couplers can transmit the excitation light to small fluorescent samples, such as cells and proteins. Also, PDMS LGP emitted about 0.5% of light's leakage to the backside, slightly higher than the simulation results due to unwanted particles on the surface (Supplementary Fig. 2).

To measure the uniformity of the extracted light around the light out-coupler, we measured the emission light from fluorescence

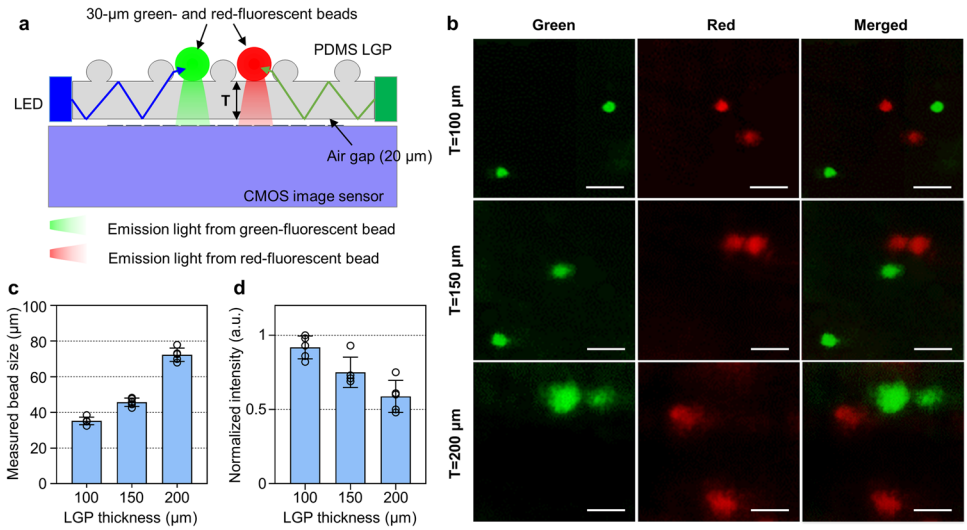

Fig. 4 Comparison of resolution and fluorescence intensity according to the thickness of the PDMS LGP for observing 30-μm green- and red-fluorescent beads. a Schematic diagram showing green- and red-fluorescent beads using a miniaturized multicolor fluorescence imaging system integrated with PDMS LGP, where T is the thickness of the PDMS LGP. **b** Captured images of the multicolor fluorescent beads according to the thickness of the PDMS LGP. **c** Measured bead size according to PDMS LGP thickness. **d** Normalized intensity according to PDMS LGP thickness. Data are presented as mean values +/− s.d. with individual data points (white circle; n = 5 for all data, n is the number of the measured beads). Scale bar: 100 μm (b).

samples around the light-out coupler according to the position of the fluorescence sample. Thus, we placed the PDMS LGP on the microscope, and injected 10 μm fluorescent beads on the surface of LGP (Supplementary Fig. 3a). Then, we measured the light emitted from the fluorescent beads flowing on the surface of the LGP using an inverted microscope (IX73, Olympus, Shinjuku, Tokyo) as a detector (Supplementary Fig. 3b). Based on the measured light intensity from the fluorescent beads, we analyzed the relative light intensity and variation around the light out-coupler (Supplementary Fig. 3c). We confirmed that the LGP delivered uniform light to samples on the surface within 11% of intensity variation (average light intensity of 159.3 ± 18.1) (Fig. 3d).

Packaging and characterization of the miniaturized multicolor fluorescence imaging system integrated with the PDMS LGP

To enable multicolor fluorescence imaging, we developed a miniaturized multicolor fluorescence imaging system integrated with the PDMS LGP. The proposed system is composed of (1) a CMOS image sensor without a lens (S5K4E1GA, Samsung Electronics, South Korea) to detect the light emitted from small fluorescent samples, (2) blue and green LEDs as excitation light sources (Blue and green XLamp XQ-E HI, Cree, Inc., Durham, NC, USA), (3) a $10 \times 10 \times 8\,mm^3$ chamber for containing biological samples, such as cells, and (4) a PDMS LGP for guiding the excitation light only to the fluorescent samples (Fig. 1d). The unit pixel size of the CMOS image sensor is $1.4 \times 1.4\,\mu m^2$, and the number of pixels is about 5 million ($2592 \times 1944\,\mu m^2$ of the effective pixels and about 5 mm^2 of FOV), which enables acquiring high-resolution images, i.e., images similar to the images obtained from a microscope with a 20X objective lens.

First, we attached the CMOS image sensor and LEDs on a customized printed circuit board (PCB) with electrical connections (Supplementary Figs. 4a–c). To block the light transmitted directly from the LEDs to the image sensor and to place the image sensor on the region where the excitation light was uniformly illuminated, we placed the LEDs about 5.5 mm away from the image sensor. Next, we placed the PDMS LGP on top of the CMOS image sensor, and we formed a gap between them by using a 20-μm thin PDMS sheet with four 1-mm holes as a spacer. The lower refractive index of air than that of the LGP enabled the TIR of excitation light inside the LGP, which minimized the leakage of light to the CMOS image sensor. Then, we bonded LEDs on the side of the LGP using a UV curable epoxy (Supplementary Figs. 4d-f). Also, we covered the vicinity of the LEDs with block epoxy to block the unnecessary light with a smaller angle of incidence than TIR that was emitted from the LEDs (Supplementary Fig. 4g). Finally, we attached the PDMS chamber on top of the LGP for loading cells with a cell culture medium (Supplementary Fig. 4h). The packaged imaging system enabled two-color fluorescence imaging through two-color LEDs and a single LGP, and its small size ($21 \times 36 \times 8\,mm^3$) allowed the real-time monitoring of cells in an incubator.

In the proposed system, the distance between the CMOS image sensor and fluorescent samples determines the resolution of the acquired images. Thus, we compared the imaging performance at various distances between a fluorescent sample and the CMOS image sensor of our miniaturized multicolor fluorescence imaging system by applying PDMS LGPs of various thicknesses (100 μm, 150 μm, and 200 μm) (Fig. 4a). In a lensless imaging system, it is essential to minimize the distance between the sensor and the sample because this distance determines the image resolution and intensity of light from the fluorescence samples[10]. In this study, first, we loaded 30 μm green- and red- fluorescent beads (FluoroMax, Thermo Fisher Scientific) onto the LGP of different thicknesses and acquired images with the CMOS image sensor. As expected, the experimental results showed that the size of the fluorescent beads increased according to the increase of the LGP thickness, and the acquired light intensity decreased (Fig. 4b-d). In addition, when we applied the 200-μm-thick LGP, the image of circular beads was distorted, and we could not obtain information about the exact shape, but the shape of the circular bead was close to a circle with the 100-μm-thick LGP (Fig. 4b). Also, the image of fluorescent beads in the processed images was about 10 μm larger than the actual size of the bead. i.e., 30 μm (Fig. 4c and Supplementary Fig. 5), which indicated that our miniaturized, multicolor, fluorescence imaging system enabled the detection of fluorescent samples that measured only tens of micrometers. The experimental result showed that thinner LGP leads to higher resolution with higher light intensity (Fig. 4c, d). Thinner PDMS LGP, i.e., less than 100 μm, would improve the quality of the image, but 100 μm is the minimum thickness that could be achieved with the current fabrication process due to the high flexibility of the

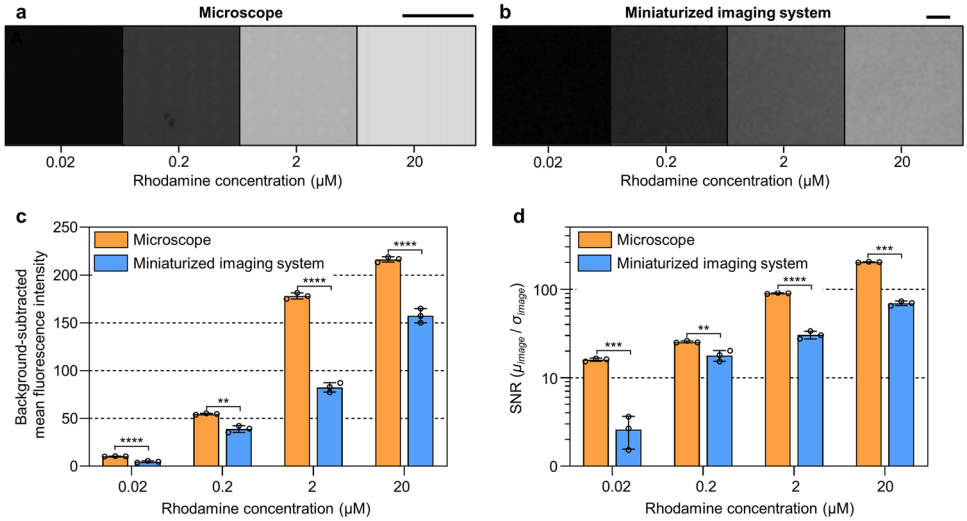

Fig. 5 Comparison of the performance of a commercial fluorescent microscope and the miniaturized imaging system integrated with a 100-μm PDMS LGP. a Background-subtracted images captured from the microscope according to rhodamine concentration (0.2-20 μM). **b** Background-subtracted images captured from the miniaturized imaging system according to rhodamine concentration (0.2-20 μM). **c** Comparison of the background-subtracted mean fluorescence intensity between the microscope and miniaturized imaging system according to rhodamine concentration (0.2-20 μM) (0.02 μM: ****P < 0.0001, 0.2 μM: **P = 0.007, 2 μM: ****P < 0.0001, 20 μM: ****P < 0.0001). **d** Comparison of the signal-to-noise ratio (SNR) between the microscope and miniaturized imaging system according to rhodamine concentration (0.2-20 μM) (0.02 μM: ***P = 0.0007, 0.2 μM: **P = 0.0016, 2 μM: ****P < 0.0001, 20 μM: ***P < 0.0002). Data are presented as mean values + /- s.d. with individual data points (white circle; n = 3 for all data, n is the number of the images). Statistical significance was tested with two-tailed unpaired t-tests. *P < 0.05; **P < 0.01; ***P < 0.001; ****P < 0.0001; NS: no significant difference. Scale bar: 100 μm (**a**, **b**).

PDMS. For recording multicolor fluorescence signals, we turned on four blue LEDs with an applied power of 0.26 W (2.6 V, 0.1 A) to each LED as an excitation light to record the green fluorescence signal and switched the excitation light to four green LEDs with an applied power of 0.26 W (2.6 V, 0.1 A) to each LED to record the red fluorescence signal. Then, we merged the two signals to construct a multicolor fluorescence image (Fig. 4b). In this experiment, we successfully observed two-color fluorescent images with 30 μm fluorescence beads using our miniaturized multicolor fluorescence imaging system integrated with a single PDMS LGP.

Next, we compared the fluorescence intensity measured by our miniaturized multicolor fluorescence imaging system integrated with a 100-μm-thick LGP with the fluorescence intensity measured by a commercial fluorescence microscope (Zeiss Axio Observer A1, Zeiss, Oberkochen, Germany). We set the same exposure time for both systems, which is the only adjustable parameter. Also, we used Rhodamine as a fluorescent source due to its wide application as a fluorescent dye for staining in the biology field. Before the comparison, we determined the optimal exposure time of the image sensor in our system through the comparisons of both fluorescence intensity and the signal-to-noise ratios (SNRs) of the acquired signals at various exposure times of the CMOS image sensor. As expected, the measured light intensity increased linearly according to its exposure time (Supplementary Figs. 6a-b). And the measured SNRs at various exposure times showed similar values, but the SNR at the exposure time of 120 ms, the maximum set exposure time, showed a slightly higher value (Supplementary Fig. 6c). Thus, we decided on the exposure time of 120 ms for the following experiments and compared the brightness and SNR of our miniaturized multicolor fluorescence imaging system with a commercial fluorescence microscope under the same exposure time (120 ms). We measured the fluorescence intensity from a Rhodamine solution at various concentrations and extracted background signals that were measured in a dark environment (Fig. 5a, b). Although the commercial fluorescence microscope showed higher fluorescence intensity and higher SNR, our system successfully detected the fluorescence signals from the rhodamine sample of 0.02 μM concentration with sufficient SNR (Fig. 5c, d).

In summary, our miniaturized multicolor fluorescence imaging system integrated with a single LGP could observe fluorescent samples, and the proposed system enabled imaging of multiple colors without additional fluorescence filters. In addition, the light intensity and SNR of our miniaturized multicolor fluorescence imaging system linearly increased according to the fluorescent intensity.

Real-time multicolor fluorescent imaging of green- and red-labeled cells

The main advantage of our system is the ability to observe multicolor fluorescence imaging through a single LGP, which made the system small enough to be located inside an incubator. Taking advantage of these features, we monitored live NIH 3T3 fibroblast cells labeled by CellTracker Green CMFDA and CellTracker Red CMTPX, which are widely used for observing dynamic characteristics of cells, such as cell spreading, migration, and proliferation. (The detailed culture protocol is provided in the Methods and Supplementary Fig. 7.) Also, NIH 3T3 fibroblast cells are commonly used in biological studies, e.g., for the observation of various dynamic characteristics. After seeding green- and red-labeled NIH 3T3 fibroblast cells on the top surface of our PDMS LGP (Fig. 6a), we continuously observed cell movement and physical changes on the PDMS LGP with an air gap. For the observation of cells inside an incubator, we located the system seeded with cells and connected the system with a laptop computer through a cable for acquiring images. For observing multicolor fluorescence images, we selectively turned on four blue LEDs with applied power 0.26 W (2.6 V, 0.1 A) to each LED for excitation of green fluorescent samples and four green LEDs with an applied power of 0.26 W (2.6 V, 0.1 A) to each LED for excitation of red fluorescent samples. We enabled automatic measurement of fluorescent signals every 4 minutes using AutoScreenShot (open-source capture program). The reflective index of the culture medium (n = ~1.33) in the chamber is higher than that of air (n = 1) before injecting the medium. Nevertheless, the TIR condition was still maintained because the reflective index of PDMS LGP (n = 1.4) is higher than that of the medium. Thus, we

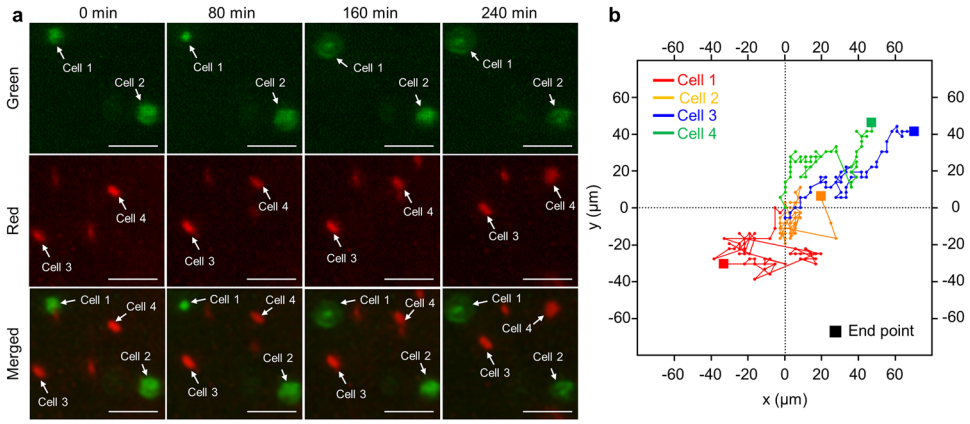

Fig. 6 Real-time monitoring of the green- and red-labeled NIH 3T3 fibroblast cells in an incubator using the miniaturized multicolor fluorescence imaging system and migration of each labeled cell over time. a Migration of the green- and red-labeled NIH 3T3 fibroblast cells over time. **b** Change of position of each cell over time. Scale bar: 100 μm (**a**).

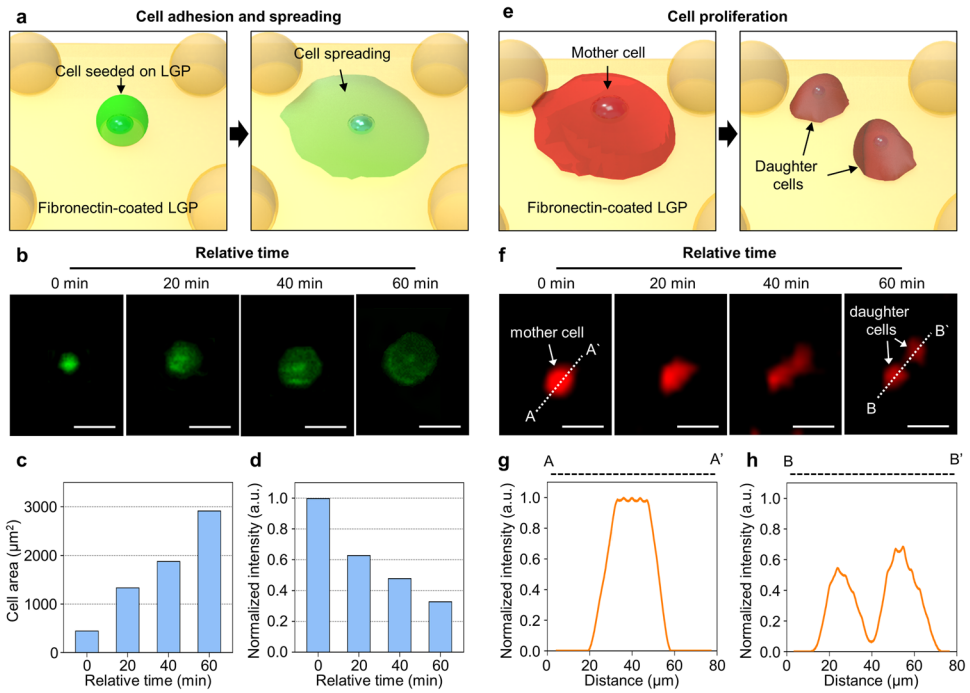

Fig. 7 Dynamic characteristics of green- and red-labeled NIH 3T3 fibroblast cell. a Schematic diagram of the spreading of a labeled cell on PDMS substrate coated with fibronectin. **b** Dynamic images of a labeled cell during the spreading process. **c** Changes in cell area by cell spreading. **d** Changes in measured intensity by cell spreading. **e** Schematic diagram of labeled cell proliferation on PDMS substrate coated with fibronectin. **f** Dynamic images of a labeled cell during the proliferation process. One mother cell was divided into two daughter cells. **g** Cross-section intensity of the mother cell before cell proliferation. **h** Cross-section intensity of the daughter cells after cell proliferation. Scale bar: 100 μm (**b**, **f**).

successfully observed the emitted light from the labeled cells (Supplementary Figs. 8-9).

During the continuous observation of cells, we successfully observed slow cell migrations (Fig. 6a and Supplementary Video 1). From the time-lapsed images acquired by the image sensor for 5 h (Fig. 6b), we were able to calculate the average migration speed of the cells, which was 20.77 ± 6.71 μm·h^{-1}, which was lower than the maximum speed (~40 μm·h^{-1}) of NIH 3T3 fibroblast cells on a patterned polyurethane-acrylate (PUA) surface and similar to the previously reported average speed (~16 μm·h^{-1})[25]. Thus, we confirmed that we successfully observed the migration of both green- and red-labeled NIH 3T3 fibroblast cells using our miniaturized multicolor fluorescence imaging system.

Also, we were able to observe other dynamic characteristics of cells, such as spreading and proliferation. The adhesion and spreading of cells on a substrate are the initial and essential steps for cell growth (Fig. 7a). Immediately after cell seeding, we continuously monitored the size changes of green-labeled NIH 3T3 fibroblast cells. We found that the cell area's size increased by spreading the cell on a PDMS substrate coated with fibronectin (Fig. 7b). The area occupied by the cell increased from 452 μm^2 to 2920 μm^2 within 1 h (Fig. 7c), which was similar to a previously reported study[26]. However, the fluorescence intensity decreased as the cell area increased (Fig. 7d) because the cell's height decreased as the area of the cell increased. As a result, the amount of light transmitted to the cell decreased.

Finally, we found that the miniaturized multicolor fluorescence imaging system enabled observation of cell proliferation, which is essential for the developmental stage of cells (Fig. 7e). During the real-time observation of cells growing in the incubator, we found that red-labeled cells proliferated from mother cell to daughter cells (Fig. 7f and Supplementary Video 2). We successfully observed proliferation procedures and confirmed the division of the cell through line plots of fluorescence intensity from the captured images before and after proliferation (Fig. 7g, h). In conclusion, using our miniaturized multicolor fluorescence imaging system integrated with a single PDMS LGP, we were able to successfully observe in real-time the spreading, migration, and proliferation of green- and red-labeled NIH 3T3 fibroblast cells in an incubator. Such observations are difficult to achieve using a conventional fluorescence microscope.

DISCUSSION

We proposed a miniaturized multicolor fluorescence imaging system integrated with a single LGP instead of using a multiple-filter set or dual-band filter. The PDMS-based LGP integrated in the system allowed for guiding excitation lights to the fluorescent samples, thus enabling multicolor fluorescence imaging. Our approach could achieve miniaturized multicolor imaging systems with minimized optical components by eliminating the aggregation of fluorescence filter sets or expensive dual-band filter, which had been essential components for the observation of multicolor fluorescent samples. Also, the PDMS LGP with spherical light out-coupler, designed for increasing light exaction angle, provided sufficient light for the excitation of small fluorescence samples (e.g., fluorescence bead and cell). We showed that the proposed system could acquire images from the two-color fluorescent sample, and the number of colors can be extended easily to more than three colors by attaching additional LEDs with different wavelengths for the excitation of another colored-fluorescent sample. Furthermore, our small (~ 6 cm^3) packaged system enabled the real-time observation of the dynamic characteristics of live cells in the incubator, and we successfully observed the spreading, migration, and proliferation of fibroblast cells in an incubator.

Although we successfully demonstrated the useful functionality of our system in the biomedical application requiring a spatial resolution of about 10 µm, there is still room for improvement of the system and for its extension to other application areas. Specifically, the spatial resolution and SNR can be improved by applying thinner PDMS or thin glass-based LGP (Fig. 4). Reducing the distance between the image sensor and the sample can increase the spatial resolution and the amount of light delivered to the image sensor. To expand the applications of the proposed system, efforts to reduce the distance below 10 µm, including the air gap, will be required. Also, an advanced image sensor with a higher resolution can enhance the spatial resolution of the acquired image. Additionally, the application of image processing algorithms can sufficiently improve spatial resolution. For example, one of the previous studies achieved a spatial resolution of 4 µm by applying compressive decoding algorithms[15], which is equivalent to a 40x microscope image. In summary, we expect that performance improvements on the hardware (i.e., minimization of the distance between the sensor and samples or integration of advanced image sensor) and software (i.e., post-image processing algorithm) will lead to significant improvements in the resolution. Also, the integration of micro-pole patterns beneath the PDMS LGP will expand the active area (i.e., actual FOV) compared to the system that uses a PDMS sheet for forming an air gap. Also, the integration of a micro-mirror on the other side of the PDMS LGP will improve the excitation light's uniformity[22].

Furthermore, our miniaturized, multicolor, fluorescence imaging system integrated with a single LGP could be utilized for a broader range of applications than those of conventional fluorescence microscopes. For example, by simultaneously labeling several cell types from a specific organ (e.g., neuron, astrocyte, and microglia in the case of the brain), the proposed system could be used to observe the interaction among them inside a microfluidic chip integrated with the miniaturized fluorescence imaging system. Also, the proposed system can enable a small fluorescence reader for portable point-of-care testing (POCT) applications. Specifically, the microscope has been used as the reader to detect the fluorescence signals from biomarker-encoded hydrogel microparticles[18]. We expect our system to be a small fluorescent reader that replaces the microscope, allowing real-time readout in fields, not limited to the laboratory. In conclusion, we expect our fluorescence imaging platform to be utilized in various studies in the biomedical field that require multicolor fluorescence imaging capability.

METHODS

Preparation for characterizations of the PDMS LGP integrated with LEDs

To measure the angular luminance distribution of fabricated PDMS LGP, we attached four small blue XQ-E LEDs as light sources on the side of the LGP. And we fixed the PDMS LGP integrated with LEDs on a tripod. Then, we measured luminance emitted from the PDMS LGP from the top of the LGP using a CS-2000 Spectroradiometer (Konica Minolta, Osaka, Japan) by changing the angle by 5 degrees in the absence of ambient light (Fig. 3c).

In addition, to measure the uniformity of the extracted light around the light out-coupler, we used 10 µm diameter green fluorescent beads (G1000B, Thermo Fisher Scientific, Middlesex County, MA, USA), which were similar to the size of the cell as a target sample. As shown in Supplementary Figure 3, we used PDMS LGP integrated with four LEDs as light sources, and we used an inverted microscope (IX73, Olympus, Shinjuku, Tokyo) as a detector to measure the fluorescent signal emitted by the beads. We treated the surface of the PDMS LGP with oxygen plasma to maintain the hydrophilic surface, and we used a pipette to pour 2.5 µL of DI water which contained 10 µm fluorescent beads on the surface of the LGP. We applied power of 0.26 W (2.6 V, 0.1 A) to each LED using a power supply. In this experiment, the SNR was calculated by dividing the mean fluorescence intensity by the standard deviation of all pixels in the background-subtracted images[27].

Cell culture and preparation

Before cell culture on our PDMS LGP, we cleaned the LGP's top surface three times using 70% ethanol for 30 min and placed it under UV light on a clean bench for 24 h (Supplementary Fig. 7a). Next, the LGP's top surface was treated with oxygen plasma (80 W for 40 s at 50 mTorr; Covance-MP; Femto Science, South Korea) and subsequently incubated with 20 $\mu g \cdot mL^{-1}$ of fibronectin (FN; Sigma-Aldrich, St. Louis, MO, USA) for 4 h at 37 °C to enhance cell attachment[28,29] (Supplementary Fig. 7b).

To monitor the dynamic characteristics of two-color-labeled cells, we divided NIH 3T3 fibroblast cells into 1 mL aliquots in two 1.5 mL microcentrifuge tubes (Eppendorf, Enfield, CT, USA). Next, the cells were labeled with 5 $\mu mol \cdot L^{-1}$ of CellTracker Green CMFDA (5-chloromethylfluorescein diacetate) (Invitrogen, Carlsbad, CA, USA) or 5 $\mu mol \cdot L^{-1}$ of CellTracker Red CMTPX (Invitrogen) with a culture medium (Dulbecco's modified Eagle's medium [DMEM; Gibco, Gaithersburg, MD, USA] supplemented with 10% [v/v] fetal calf serum [Gibco] and penicillin-streptomycin [Gibco]) for 30 min in an incubator (Supplementary Fig. 7c). Next, the culture medium containing the dye was removed, and a fresh medium was put in each 1.5 mL microcentrifuge tube that contained the green- or red-labeled cells. The 5×10^4 green- and red-labeled cells were plated on the FN-coated PDMS LGP (Supplementary Fig. 7d).

Finally, the culture chamber was filled with a fresh culture medium at 37 °C and 5% CO_2 for cell culture.

Real-time cell imaging

To monitor the dynamic characteristics of NIH 3T3 fibroblast cells (i.e., cell spreading, migration, and proliferation) in an incubator, we observed green- and red-labeled cells using our miniaturized multicolor fluorescence imaging system. First, we connected power lines to the imaging system to supply power to the CMOS image sensor and LEDs while locating the system in the incubator. We turned on the LEDs with applied power of 0.26 W (2.6 V, 0.1 A) to each LED only at the time of observation through the regulation of the power supply to prevent photobleaching and cell damage due to the heat generated by the LEDs. Every 4 min, we obtained images of green- and red-labeled cells by blue and green exaction light with a time difference, respectively. Also, during the operation of the LEDs and the image sensor, the temperature measured near the LED and the image sensor was 28.5 °C and 28.1 °C, respectively. The temperature measured from the system was lower than the incubator temperature, and it seemed that the activity and viability of the cells were not affected.

Image processing

After observing the fluorescent beads or the green- and red-labeled cells, we processed each image. Initially, each image was split as an RGB image. Then, to selectively acquire only the emission light of the fluorescent beads or labeled cells, we extracted a split image similar to the emission light wavelength, that is, a green image was extracted to observe green fluorescent beads or green-labeled cells (Supplementary Fig. 5). Through the above process, chromatic aberration was not observed. Also, to minimize the ambient light entering the CMOS image sensor and to improve the spatial resolution, the background light was reduced by adjusting the contrast and brightness using ImageJ2 (open-source software) (Supplementary Fig. 5). We applied the same condition of contrast and brightness for all images. Finally, we merged two processed images for observing two fluorescent beads or green- and red-labeled cells. Also, we arranged the merged images in chronological order to observe the cell dynamics.

Statistical analysis

GraphPad Prism 8 software (Graphpad Software inc., USA) was used to assess the statistical significance. The differences between groups were assessed via unpaired t-tests.

Reporting summary

Further information on research design is available in the Nature Research Reporting Summary linked to this article.

DATA AVAILABILITY

All data supporting the findings of this study are available within the paper and its supplementary information files or from the corresponding author upon reasonable request.

Received: 23 September 2022; Accepted: 25 January 2023;
Published online: 09 February 2023

REFERENCES

1. Shih, H. C. et al. Microfluidic Collective Cell Migration Assay for Study of Endothelial Cell Proliferation and Migration under Combinations of Oxygen Gradients, Tensions, and Drug Treatments. *Sci. Rep.* **9**, 8234 (2019).
2. Kamada, R. et al. Effective Cellular Morphology Analysis for Differentiation Processes by a Fluorescent 1,3a,6a-Triazapentalene Derivative Probe in Live Cells. *PLoS One* **11**, e0160625 (2016).
3. Kang, S. et al. Characteristic analyses of a neural differentiation model from iPSC-derived neuron according to morphology, physiology, and global gene expression pattern. *Sci. Rep.* **7**, 12233 (2017).
4. Ah Lee, S., Ou, X., Lee, J. E. & Yang, C. Chip-scale fluorescence microscope based on a silo-filter complementary metal-oxide semiconductor image sensor. *Opt. Lett.* **38**, 1817–1819 (2013).
5. Sencan, I., Coskun, A. F., Sikora, U. & Ozcan, A. Spectral demultiplexing in holographic and fluorescent on-chip microscopy. *Sci. Rep.* **4**, 3760 (2014).
6. Pang, S., Han, C., Kato, M., Sternberg, P. W. & Yang, C. Wide and scalable field-of-view Talbot-grid-based fluorescence microscopy. *Opt. Lett.* **37**, 5018–5020 (2012).
7. Jin, D. et al. Compact Wireless Microscope for In-Situ Time Course Study of Large Scale Cell Dynamics within an Incubator. *Sci. Rep.* **5**, 18483 (2015).
8. Coskun, A. F., Su, T. W. & Ozcan, A. Wide field-of-view lens-free fluorescent imaging on a chip. *Lab Chip* **10**, 824–827 (2010).
9. Greenbaum, A. et al. Imaging without lenses: achievements and remaining challenges of wide-field on-chip microscopy. *Nat. Methods* **9**, 889–895 (2012).
10. Coskun, A. F., Sencan, I., Su, T. W. & Ozcan, A. Lensless wide-field fluorescent imaging on a chip using compressive decoding of sparse objects. *Opt. express* **18**, 10510–10523 (2010).
11. Shanmugam, A. & Salthouse, C. Lensless fluorescence imaging with height calculation. *J. Biomed. Opt.* **19**, 16002 (2014).
12. Martinelli, L. et al. Sensor-integrated fluorescent microarray for ultrahigh sensitivity direct-imaging bioassays: Role of a high rejection of excitation light. *Appl. Phys. Lett.* **91**, 083901 (2007).
13. Coskun, A. F., Sencan, I., Su, T. W. & Ozcan, A. Lensfree Fluorescent On-Chip Imaging of Transgenic Caenorhabditis elegans Over an Ultra-Wide Field-of-View. *PLoS One* **6**, e15955 (2011).
14. Mudraboyina, A. K., Blockstein, L., Luk, C. C., Syed, N. I. & Yadid-Pecht, O. A Novel Lensless Miniature Contact Imaging System for Monitoring Calcium Changes in Live Neurons. *IEEE Photonics J.* **6**, 1–15 (2014).
15. Coskun, A. F., Sencan, I., Su, T. W. & Ozcan, A. Wide-field lensless fluorescent microscopy using a tapered fiber-optic faceplate on a chip. *Analyst* **136**, 3512–3518 (2011).
16. Zellner, M. et al. Fluorescence-based Western blotting for quantitation of protein biomarkers in clinical samples. *Electrophoresis* **29**, 3621–3627 (2008).
17. Chinen, A. B. et al. Nanoparticle Probes for the Detection of Cancer Biomarkers, Cells, and Tissues by Fluorescence. *Chem. Rev.* **115**, 10530–10574 (2015).
18. Yeom, S. Y. et al. Multiplexed Detection of Epigenetic Markers Using Quantum Dot (QD)-Encoded Hydrogel Microparticles. *Anal. Chem.* **88**, 4259–4268 (2016).
19. Pang, S., Han, C., Erath, J., Rodriguez, A. & Yang, C. H. Wide field-of-view Talbot grid-based microscopy for multicolor fluorescence imaging. *Opt. Express* **21**, 14555–14565 (2013).
20. Kuhnemund, M. et al. Targeted DNA sequencing and in situ mutation analysis using mobile phone microscopy. *Nat. Commun.* **8**, 13913 (2017).
21. Lee, J., Yeon, J., Kim, K. & Yoon, J. Mass-Producible Polydimethylsiloxane (PDMS) Frontlight Unit (FLU) for Reflective Displays. *J. Disp. Technol.* **7**, 526–531 (2011).
22. Lee, J. H. et al. Design and fabrication of a micropatterned polydimethylsiloxane (PDMS) light-guide plate for sheet-less LCD backlight unit. *J. Soc. Inf. Disp.* **16**, 329–335 (2008).
23. Guertin, D. A. & Sabatini, D. M. Cell Size Control. In eLS, (Ed.). https://doi.org/10.1038/npg.els.0003359 (2006).
24. Lee, J.-H., Choi, W.-S., Lee, K.-H. & Yoon, J.-B. A simple and effective fabrication method for various 3D microstructures: backside 3D diffuser lithography. *J. Micromech. Microeng.* **18**, 125015 (2008).
25. Kim, D. H. et al. Mechanosensitivity of fibroblast cell shape and movement to anisotropic substratum topography gradients. *Biomaterials* **30**, 5433–5444 (2009).
26. Huang, C. K. & Donald, A. Revealing the dependence of cell spreading kinetics on its spreading morphology using microcontact printed fibronectin patterns. *J. R. Soc. Interface* **12**, 20141064 (2015).
27. Ferrand, A., Schleicher, K. D., Ehrenfeuchter, N., Heusermann, W. & Biehlmaier, O. Using the NoiSee workflow to measure signal-to-noise ratios of confocal microscopes. *Sci. Rep.* **9**, 1165 (2019).
28. Toworfe, G. K., Composto, R. J., Adams, C. S., Shapiro, I. M. & Ducheyne, P. Fibronectin adsorption on surface-activated poly(dimethylsiloxane) and its effect on cellular function. *J. Biomed. Mater. Res A* **71a**, 449–461 (2004).
29. Zhang, W. J., Choi, D. S., Nguyen, Y. H., Chang, J. & Qin, L. D. Studying Cancer Stem Cell Dynamics on PDMS Surfaces for Microfluidics Device Design. *Sci. Rep.* **3**, 2332 (2013).

ACKNOWLEDGEMENTS

This work was supported by Institute of Information & communications Technology Planning & Evaluation (IITP) grant funded by the Korea government (MSIT) (No. 2021-0-00538). This work was also supported by the Brain Convergence Research Program of the National Research Foundation (NRF) funded by the Korean government (MSIT)

(NRF-2019M3E5D2A01063814) and the Research program for understanding and regulation of brain function of the National Research Foundation (NRF) funded by the Korean government (MSIT) (NRF-2022M3E5E8081196). This work was also supported by the Institute for Basic Science (IBS), Center for Cognition and Sociality (IBS-R001-D1-2023-a02) and Korea University intramural grant.

AUTHOR CONTRIBUTIONS

H.S. and G.-W.Y. performed most of the experiments, analysed the data, prepared the figures, and wrote the manuscript. G.-W.Y. designed, fabricated and characterized the PDMS light-guide plate. H.S. designed, fabricated and characterized the miniaturized multicolor fluorescence imaging system. H.S. performed In vitro experiment. W.C. was involved in preparing the system's characterization. D.L., H.C., and J.D.S. discussed the results and provided comments. N.C., J.-B.Y. and I.-J.C. discussed the results, provided comments, and wrote the manuscript. All of the authors reviewed the manuscript.

COMPETING INTERESTS

The authors declare no competing interests.

ADDITIONAL INFORMATION

Supplementary information The online version contains supplementary material available at https://doi.org/10.1038/s41528-023-00243-6.

Correspondence and requests for materials should be addressed to Nakwon Choi, Jun-Bo Yoon or Il-Joo Cho.